ELSEVIER

Surface Science 331–333 (1995) 1422–1429

surface science

Anharmonic thermal vibrations observed by surface X-ray diffraction for Cs/Cu(001)

H.L. Meyerheim [a,*], W. Moritz [a], H. Schulz [a], P.J. Eng [b], I.K. Robinson [b]

[a] *Institut für Kristallographie und Mineralogie, Universität München, Theresienstrasse 41, D-80333 München, Germany*
[b] *Department of Physics, University of Illinois, Urbana, IL 61801, USA*

Received 3 August 1994; accepted for publication 11 November 1994

Abstract

Surface X-ray diffraction measurements at 190 and 303 K have been used to analyse the thermal disorder of an uniaxial incommensurate quasi-hexagonal Cs-monolayer on Cu(001). Within the harmonic vibration model a Debye-like thermal behaviour is found for the mean square vibration amplitudes U^{ii} ($i = 1,2$) of the Cs-atoms along the [100] ($i = 1$) and the [010] ($i = 2$) direction, where the adsorbate structure is commensurate and incommensurate with the substrate, respectively. At 190 K we determine $U^{11} = 0.10(2)$ Å^2 and $U^{22} = 0.16(2)$ Å^2, at 303 K $U^{11} = 0.18(2)$ Å^2 and $U^{22} = 0.29(3)$ Å^2. From this temperature dependence Debye temperatures of $\Theta_{[100]} = 45$ K and $\Theta_{[010]} = 35$ K are derived which are comparable with the bulk Cs-Debye temperature of 38 K. A significant better agreement between calculated and observed structure factors is obtained by taking account of anharmonic contributions to the thermal disorder using the Gram–Charlier series expansion of the harmonic (Gaussian) probability density function. Besides a larger width of the probability density function along [100] and [010] the derived anharmonic probability density function exhibits a stronger anisotropy as compared to its harmonic counterpart. The shape of the anharmonic probability density function can directly be correlated to the geometry of the Cs-overlayer structure. At 190 K this is most evident by a small width of the anharmonic probability density along [110], where the Cs-atoms are arranged in a densely packed chain. At 303 K the anisotropy is less pronounced indicating isotropisation close to the break down of the structure at 328 K.

Keywords: Alkali metals; Copper; Single crystal surfaces; Surface structure

1. Introduction

The detailed knowledge of the crystal structure is of fundamental interest in many branches of solid state science, since it controls many properties of crystalline matter. In addition to the determination of the equilibrium atomic coordinates precise information about the static and dynamic disorder is a prerequisite for a complete understanding of the crystal structure. The thermal vibration of the atoms is one of the most prominent examples for structural details which in X-ray diffraction (XRD) generally is taken into account using the harmonic model, i.e. by a Gaussian probability density function (PDF) of the atoms. However, thermal expansion and the limited thermal conductivity in insulators or third order elastic constants are direct manifestations of anharmonicity. Since the early work of Waller [1] a huge amount of theoretical and experimental work has been per-

* Corresponding author.

SSDI 0039-6028(95)00199-9

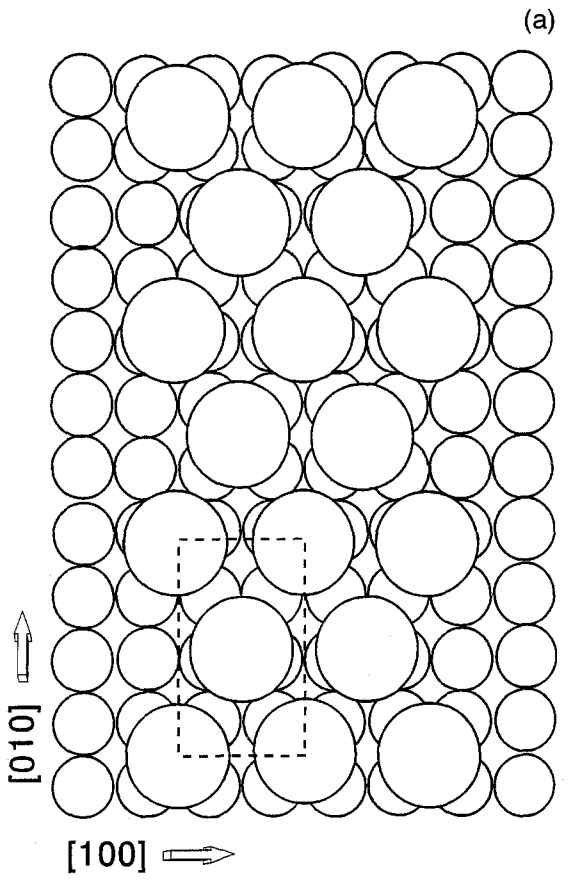

formed investigating the effect of anharmonic vibrations on the Bragg and diffuse scattering. More details can be found in Refs. [2–6].

In contrast, little work has been performed on the analysis of anharmonic vibrations on crystal surfaces, although in this case these are expected to be even more important than in the bulk. For example, enhanced anharmonicity on surfaces has been observed by surface-extended X-ray absorption fine structure (SEXAFS) measurements and by energy-resolved He-scattering data [7,8]. On the other hand, well established long range order techniques like low energy electron diffraction (LEED) and surface XRD [9,10] still use the harmonic approximation only allowing for isotropic or anisotropic vibrations.

On the basis of surface XRD data we demonstrate in this work the importance of anharmonic vibrations within a densely packed quasi-hexagonal Cs-monolayer adsorbed on atomically clean Cu(001). The derived PDFs of the Cs-atoms indicate enhanced vibration amplitudes and stronger anisotropy as compared to the harmonic (Gaussian) PDF. The shape of the anharmonic PDFs and the calculated one particle potentials (OPPs) are related to the quasi-hexagonal geometry of the adsorbate structure.

2. Results and discussion

The experiments were performed at the beamline X16A of the National Synchrotron Light Source (NSLS) in Brookhaven, USA, using the UHV diffractometer described by Fuoss et al. [11]. Cs was evaporated on atomically clean Cu(001) at 190 and 303 K from thoroughly degassed SAES getter sources. More details have been discussed in Ref. [12].

Fig. 1. (a) Structure of Cs/Cu(001)-c(2×10) at about 0.3 ML. The Cs- and Cu-atoms are represented by large and small circles, respectively. The adsorbate unit cell used for the structure refinement is shown by the dashed rectangle. (b) Measured structure factor amplitudes $|F_{hk0}^{obs}|$ represented by the radii of the semicircles for 190 K (left semicircle) and 303 K (right semicircle). The data sets are scaled to the (020) reflection.

The Fig. 1a shows the commensurate quasi-hexagonal c(2 × 10) superstructure that forms after completion of the Cs-adlayer at 0.30 monolayers (ML) coverage, where 1 ML corresponds to 1.53×10^{15} atoms cm^{-2}. Large circles represent Cs-atoms, small circles Cu-atoms. The adlayer registry relative to the substrate has been determined by the intensity analysis of the integer order truncation rods [10,12]. Variation of the Cs-coverage leads to the formation of an uniaxially incommensurate superstructure, where the incommensurability is observed along the [010] direction (b-axis).

The superstructure unit cell chosen for the present analysis is indicated by the dashed rectangle. Our previous surface XRD investigations have proven the effective substrate corrugation potential to be small as compared to the Cs–Cs dipole interaction potential (~ 40 meV versus 1 eV) [12,13]. Therefore to first order the influence of the substrate surface can be neglected and the choice of the unit cell is justified. In addition, the variation of the adlayer density leads to a continuous expansion and contraction of the adlayer along the b-axis rather than to the spontaneous formation of domain walls during the transition from the commensurate to the incommensurate phase. This has been deduced from reflection profile analysis [14] which does not exhibit a change as a function of incommensurability. Consequently, the Cs-overlayer can be viewed as a floating solid [15] representing a nearly ideal two-dimensional crystal.

The measured structure factor amplitudes $|F^{obs}_{hk0}|$ of the fractional order Cs-superlattice reflections are represented by the radii of the semicircles shown in Fig. 1b for 190 and 303 K. In general, two symmetry equivalent reflections have been measured for deriving each structure factor amplitude, the reproducibility being in the 10% regime. After correcting the measured intensity data for active sample area, polarisation- and Lorentz-factor [10], in total 13 and 11 symmetrically independent in-plane structure factor amplitudes $|F^{obs}_{hk0}|$ were obtained at 190 and 303 K, respectively. The experimental uncertainty σ_{hk} was estimated by the quadrature sum of the statistical and systematic errors [10]. Since only two Cs-atoms at (0,0) and (1/2,1/2) are located in the surface unit cell, all F^{obs}_{hk0} are real and positive.

It is important for the present analysis that no atomic coordinates have to be refined, thus leaving the temperature factor $T(\boldsymbol{h})$ the only fit parameter. In the first step the data were fitted allowing for anisotropic harmonic (subscript H) vibrations which

Table 1
List of measured (F^{obs}) and calculated (F^{calc}) structure factors using harmonic (H) and anharmonic (A) thermal parameters; the refinement results and the agreement parameters are given below

h	k	F^{obs}	F^{calc}_H	$\lvert\Delta F/\sigma\rvert_H$	F^{calc}_A	$\lvert\Delta F/\sigma\rvert_A$
Temperature = 190 K						
0	2	100.0	91.1	0.69	87.4	0.97
0	4	48.6	42.6	1.09	44.8	0.68
0	6	24.8	13.7	2.01	21.6	0.58
1	1	89.9	98.6	0.95	99.4	1.03
1	3	56.0	58.6	0.47	55.4	0.09
1	5	25.7	23.0	0.74	28.0	0.62
2	2	54.1	57.5	0.46	55.9	0.24
2	4	24.8	28.6	1.40	26.3	0.57
3	1	53.2	41.3	2.58	48.5	1.03
3	3	22.0	26.4	1.19	21.8	0.06
4	2	18.3	18.3	0.01	20.1	0.64
4	4	7.3	9.6	0.62	4.3	0.83
3	5	9.2	11.1	0.68	9.0	0.08
R_u			12.7%		8.5%	
R_w			15.5%		8.6%	
GOF			1.4		0.8	
U^{11}			0.10(2) Å^2		0.07(2) Å^2	
U^{22}			0.16(2) Å^2		0.22(4) Å^2	
D^{1111}			–		$0.07(5)\times10^{-4}$	
D^{2222}			–		$0.22(4)\times10^{-4}$	
D^{1122}			–		$-0.11(3)\times10^{-4}$	
Temperature = 303 K						
0	2	100.0	93.5	1.27	99.7	0.08
0	4	33.0	28.9	2.11	32.2	0.42
0	6	3.9	4.6	0.17	6.4	0.64
1	1	105.7	104.8	0.18	106.7	0.11
1	3	42.7	47.3	2.37	43.0	0.09
1	5	10.0	10.6	0.27	11.6	0.72
2	2	41.5	45.1	0.79	41.4	0.02
3	1	29.7	25.7	1.31	30.1	0.12
3	3	11.2	12.4	0.50	11.2	0.04
4	2	6.5	6.4	0.03	5.6	0.32
4	4	8.2	2.2	1.33	1.3	1.55
R_u			8.2%		3.7%	
R_w			9.4%		4.2%	
GOF			1.4		0.8	
U^{11}			0.18(2) Å^2		0.41(5) Å^2	
U^{22}			0.29(3) Å^2		0.44(6) Å^2	
D^{1111}			–		$7.0\ (3.0)\times10^{-4}$	
D^{2222}			–		$0.5\ (3)\times10^{-4}$	
D^{1122}			–		–	

are represented by a probability density function (PDF) according to:

$$\mathrm{PDF}_{\mathrm{H}}(\boldsymbol{u}) = \frac{\sqrt{\det P}}{(2\pi)^{3/2}} \mathrm{e}^{-(1/2)u^{\mathrm{T}}Pu}, \qquad (1)$$

where the vector $\boldsymbol{u}$ represents the displacement from the equilibrium position with $\boldsymbol{P} = \boldsymbol{U}^{-1}$ and $\boldsymbol{U} = \langle \boldsymbol{u}\boldsymbol{u}^{\mathrm{T}} \rangle$. The brackets $\langle\ \rangle$ indicate time and ensemble average [2]. The $\mathrm{PDF}_{\mathrm{H}}(\boldsymbol{u})$ is the Fourier transform of the temperature factor $T_{\mathrm{H}}(\boldsymbol{h})$ which is expressed by

$$T_{\mathrm{H}}(\boldsymbol{h}) = \mathrm{e}^{-2\pi^2 h_i |a_i^*| h_j |a_j^*| U^{ij}}, \qquad (2)$$

with h_i representing the covariant reflection indices and $\boldsymbol{a}_i^*$ the reciprocal cell axes. The reciprocal lattice vector $\boldsymbol{h}$ is then given by $\boldsymbol{h} = h_i \boldsymbol{a}_i^*$, using the sum convention over $i = 1,2$. Due to the mm2 site symmetry of the Cs-atoms only the diagonal terms U^{ii} are retained [16]. The calculated structure factors $F_{\mathrm{H}}^{\mathrm{calc}}$ and the relative deviations $|F_{\mathrm{H}}^{\mathrm{calc}} - F^{\mathrm{obs}}|/\sigma = |\Delta F/\sigma|$ are listed in Table 1 for both data sets. The F_{hk0}^{obs} are normalised to $F_{200}^{\mathrm{obs}} = 100$.

A plot of the mean square amplitudes U^{11} and U^{22} determined for the Cs-vibrations along the [100] and the [010] directions, is shown in Fig. 2 as a function of temperature. From the relation $U = 3\hbar^2 T/(mk\Theta^2)$ we can estimate Debye temperatures of $\Theta_{[100]} = 45$ K and $\Theta_{[010]} = 35$ K, where m and k represent the mass of the Cs-atom and the Boltzmann constant, respectively.

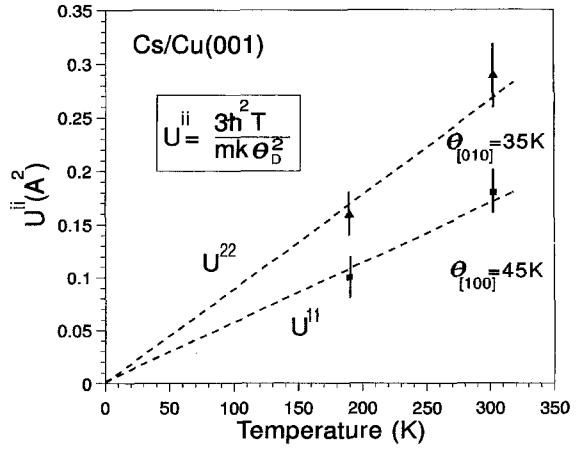

Fig. 2. Mean square displacements $U^{ii} = \langle u^i u^i \rangle$ $(i = 1,2)$ along the [100] and the [010] direction as derived on the basis of the harmonic refinement. From the slope of the lines Debye temperatures of 45 K along [100] and 35 K along [010] are estimated.

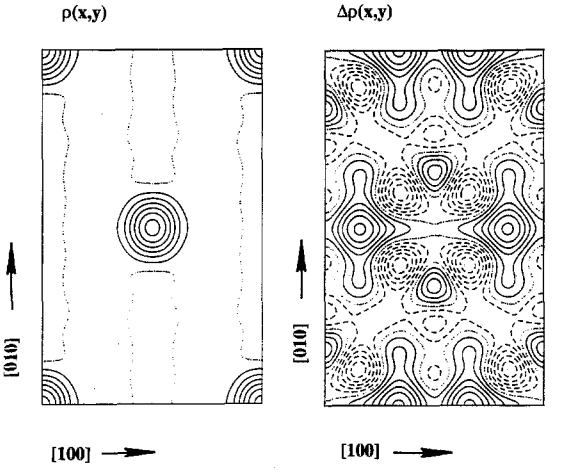

Fig. 3. Fourier synthesis $\rho(x,y)$ (left) and Difference Fourier synthesis $\Delta\rho(x,y)$ (right) for Cs/Cu(001) at 190 K on the basis of the harmonic approximation. One unit cell as indicated by the dashed lines in Fig. 1a is shown. Solid and dashed lines represent positive and negative densities, respectively. The contour line spacing used for $\Delta\rho(x,y)$ is ten times smaller than for $\rho(x,y)$.

However, the harmonic approximation is not sufficient to accurately describe the thermal motion. On the one hand this can be suspected by looking at the agreement parameters derived for the harmonic refinement (see Table 1). Both, the weighed (R_{w}) and the unweighed (R_{u}) residuals as well as the "goodness of fit" (GOF) [17] still have unsatisfactorily high values, especially in view of the simple geometric structure of the system. More importantly, direct evidence for an incomplete treatment of the thermal disorder is given by the difference Fourier synthesis of the harmonic refinement (F_{hk0}^{calc}) versus the observed data (F_{hk0}^{obs}). It is given by

$$\Delta\rho(x,y) = \sum_{h,k} \left(F_{hk0}^{obs} - F_{hk0}^{calc}\right) \cos\left[2\pi(hx + ky)\right]. \qquad (3)$$

Positive (negative) densities in the difference function $\Delta\rho(x,y)$ indicate where extra electron density $\rho(x,y)$ has to be added (removed) in order to improve the structure model [10]. Both, the Fourier synthesis $\rho(x,y)$ using F_{hk0}^{obs} and the difference Fourier synthesis $\Delta\rho(x,y)$ are shown in Fig. 3 within the centred unit cell indicated in Fig. 1a. For

$\Delta\rho(x,y)$ a ten times smaller spacing between the contour lines is used. In the difference Fourier synthesis pronounced positive (solid lines) and negative (dashed lines) maxima are observed.

Within the harmonic approximation a more detailed description of the structure is not possible; anharmonic contributions to the $\mathrm{PDF_H}(\boldsymbol{u})$ have to be considered. Anharmonic thermal vibrations were included by using the Gram–Charlier (GC) series expansion of the harmonic $\mathrm{PDF_H}(\boldsymbol{u})$ [2]:

$$\mathrm{PDF_{GC}}(\boldsymbol{u}) = \mathrm{PDF_H}(\boldsymbol{u})\left[1 + \frac{1}{3!}c^{jkl}H_{jkl}(\boldsymbol{u}) + \frac{1}{4!}c^{jklm}H_{jklm}(\boldsymbol{u}) + \ldots\right]. \quad (4)$$

The multidimensional Hermite polynomials $H_{jklm\cdot r}(\boldsymbol{u})$ are the rth order derivatives of the $\mathrm{PDF_H}(\boldsymbol{u})$ with respect to $\boldsymbol{u}$ [18]. The Fourier transform of Eq. (4) is exactly known leading to a generalised temperature factor which is included in the structure refinement program "Prometheus" [5,19]:

$$T_{\mathrm{GC}}(\boldsymbol{h}) = T_{\mathrm{H}}(\boldsymbol{h})\left[1 + \frac{(2\pi i)^3}{3!}C^{jkl}h_jh_kh_l + \frac{(2\pi)^4}{4!}D^{jklm}h_jh_kh_lh_m + \ldots\right], \quad (5)$$

where the h_j are the reflection indices.

The first and second order terms of the series expansion are set to zero, meaning that the average value and the standard deviation of the harmonic part include the anharmonic first and second order contributions. Therefore, in the case of higher order refinement, the harmonic fitparameters loose their direct interpretation as the mean atomic position and its standard deviation [2].

By symmetry all third order terms C^{ijk} vanish and only the fourth order terms D^{1111}, D^{2222} and D^{1122} can be different from zero in the present case.

The refinement including the anharmonic contributions significantly improves the fit quality for both data sets as can be seen on the right part of Table 1. It is very important to note that also the GOF parameter is improved although the anharmonic refinement increases the number of refinement parameters. This is a strong indication that the better fit quality is statistically significant. Another indication for the significance of the fit results comes from the observation that the agreement between F^{obs}_{hk0} and F^{calc}_{hk0} is improved for all reflections where major disagreements $|\Delta F/\sigma|$ have been observed for the harmonic refinement. However, the most important hint that the consideration of anharmonic terms is physically justified is given by the calculated PDFs which are shown in Fig. 4 for both, the harmonic (left) and the anharmonic (right) refinement. All PDFs are shown on the same logarithmic scale in order to emphasise the fine details. Three results are directly evident:

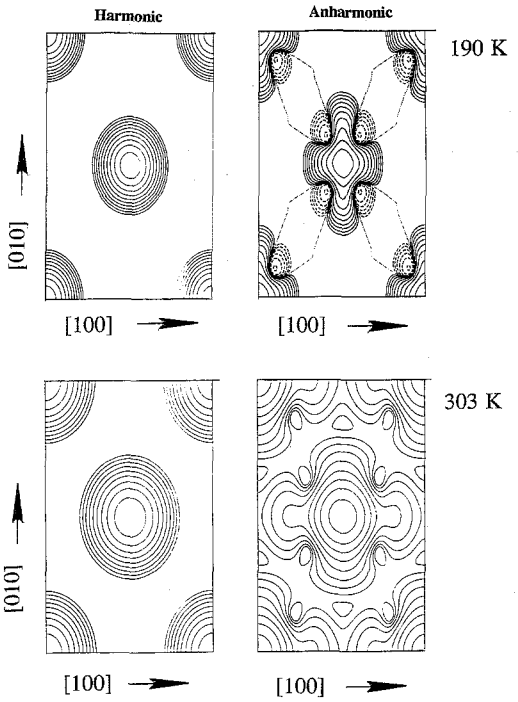

Fig. 4. Probability density functions (PDFs) within the unit cell as derived for the harmonic (left) and anharmonic (right) refinement for the 190 K (upper panel) and 303 K (lower panel) sample. The PDFs are shown on a logarithmic scale.

(i) For both temperatures there is a larger delocalisation of the anharmonic PDF along the [100] and the [010] direction as compared to the harmonic PDFs. Especially for the 303 K sample there is a finite density along [100] in between the Cs-equilibrium positions. This can be interpreted by a large mobility of the Cs-atoms along the [100] direction.

(ii) The anharmonic PDFs are characterised by a pronounced anisotropy which cannot be properly represented by the Gaussian PDFs in the harmonic approximation. It is the anisotropy which is the most prominent effect of anharmonicity in the present case. On the basis of this result the appearance of negative regions along the ⟨110⟩ directions in the difference Fourier synthesis (dashed lines in Fig. 3) can be directly understood since they are due to the excess electron density which is "created" in this regime by the harmonic temperature factor.

(iii) The shape of the anharmonic PDFs can be directly related to the geometry of the overlayer structure. Along the ⟨110⟩ directions, where the width of the anharmonic PDF is at a minimum, the Cs-atoms form linear densely packed chains with a Cs–Cs distance as low as 4.85 Å. This is about 8% (!) smaller than in bulk Cs (5.24 Å). Consequently, the Cs–Cs-interaction which to first order is dominated by the repulsive dipole–dipole potential ($V_{\mathrm{dip}} \propto r^{-3}$) is strongest along ⟨110⟩, but less important along the other directions.

Although the ratio N/P between the number of reflections (N) and the number of refinement parameters (P) is only approximately three, which is comparatively low as compared to usual surface XRD studies, the standard deviations obtained for the thermal parameters are generally in the 50% regime. This indicates a still sufficient overdetermination of the fit problem. In addition, the basic shape of the harmonic PDFs could be derived by using 9 reflections only. However, for the 303 K data set, the thermal parameter D^{1122} was found not to be significant (standard deviation ~ 100%) and was therefore not included in the refinement. This can be explained by the reduced anisotropy of the PDF at high temperature close to the breakdown of the superstructure which is observed at about 328 K under the present conditions [13,14].

The calculation of the effective one-particle potential (OPP) [5], according

$$V(\boldsymbol{u}) = -kT \ln\left[\frac{\mathrm{PDF}(\boldsymbol{u})}{\mathrm{PDF}(\boldsymbol{u}=\boldsymbol{u}_0)}\right], \qquad (6)$$

is shown in Fig. 5 for the [100], [010] and the [110] directions. In Eq. (6) the vectors $\boldsymbol{u}_0$ and $\boldsymbol{u}$ represent the equilibrium position and the displacement from

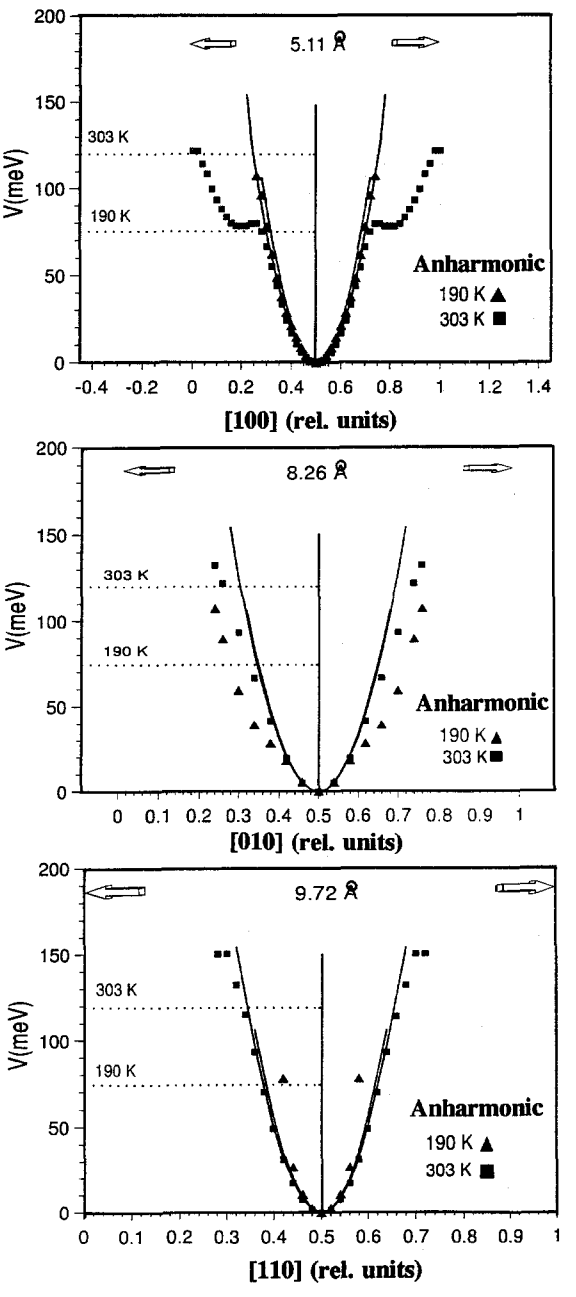

Fig. 5. Effective one-particle potentials within one unit cell along the [100], [010] and the [110] direction. The arrows indicate the lengths of the section through the unit cell; the length scale along the abscissa is given in relative units. The harmonic potentials are represented by the solid lines; the anharmonic potentials by triangles and squares for the 190 and 303 K measurement, respectively. The absolute length scale is identical for all plots.

it. The parameter k is the Boltzmann constant, T the absolute temperature. Solid lines represent the OPPs calculated for the harmonic approximation; squares and triangles indicate sampling points through the anharmonic OPPs for 303 and 190 K, respectively. The absolute length scale along the abscissae is identical in all plots.

For the interpretation of the potentials shown in Fig. 5 the occupation of the energy states has to be taken into account. At low temperatures only a few atoms have a high energy, therefore the potential is not well determined at points far away from the equilibrium position $\boldsymbol{u}_0$. The reliability of such parts of the potential improves with increasing temperature. Consequently, only those parts of the potential can be compared for which the energy states are sufficiently occupied at different temperatures. A rough estimation of the occupation is given by the Bose–Einstein-distribution. In Fig. 5 we have indicated by dotted horizontal lines the energy levels (~ 75 and 120 meV) which are occupied by a probability of 0.01 at 190 and 303 K. Within the comparable energy range ($E \leq 75$ meV) the calculated OPPs along the [100] direction are independent of temperature, indicating that the results are physically meaningful, although the fine details of the PDFs and the corresponding potential curves are subject to truncation errors and the limited accuracy of the data. For displacements below about 0.2 lattice units (~ 1 Å) the potentials are parabolic, indicating harmonic vibrations. In contrast, the situation is different at 303 K, where a strong deviation from a parabolic potential is observed for larger displacements. This is directly correlated to the finite density between the Cs-equilibrium positions in the anharmonic PDF at 303 K (see Fig. 4, lower right part). This result can be interpreted by a high mobility of the Cs-atoms along the [100] direction. A similar deviation from a harmonic potential has been observed for Li^+ ions in the fast ionic conductor Li_3N [20]. The high Cs-mobility along [100] can be interpreted by a diffusion mechanism where Cs-atoms change sites into vacancies located in neighbouring unit cells. In principle, other mechanisms could also be accounted for the significant Cs-delocalisation such as a direct site exchange of two Cs-atoms. However, as in the bulk, mechanisms other than vacancy site diffusion are expected to be much less important due to their much larger activation energy, especially if there is a repulsive interaction between the adsorbed atoms [21,22].

Model calculations of the activation energy assuming only a vacancy diffusion mechanism and taking account for the Cs–Cs dipole–dipole interaction, Pauli-repulsion and the substrate corrugation potential are within 20% in quantitative agreement with the experimentally derived diffusion barrier of about 120 meV [13]. Further, along other directions no such large Cs-mobility can be expected. This is due to steric reasons resulting from the larger repulsive interactions between the diffusing atom and the nearest neighbours along the diffusion path. Qualitatively, this is directly evident by inspection of the structure model shown in Fig. 1. The high mobility of the Cs-adatoms is possible only along [100], since it is favoured by the large separation of the Cs-chains in the [010] direction.

The OPPs along [010] and [110] are shown in the centre and lower panel of Fig. 5. Significant deviations from the harmonic potential are observed along [010] as well as a temperature dependency of the potentials. The latter is indicative for static disorder which has been analysed previously [12].

In summary, using surface XRD we have given evidence for the importance of anharmonic contributions to the thermal vibrations of the Cs-atoms within a close-packed quasi-hexagonal overlayer. The most prominent effect of anharmonicity is the larger anisotropy of the anharmonic PDF as compared to its harmonic counterpart. The shape of the anharmonic PDF is directly related to the geometry of the overlayer structure.

Acknowledgements

The support by the Bundesministerium für Forschung und Technologie under Grant No. 0464IAB8 is gratefully acknowledged. Work at the NSLS is supported by the US Department of Energy under DE-AC 012-76CH0016. Partial support also came from the University of Illinois Materials Lab. under DEFG02-91ER45439. One of us (H.L.M.) wants to thank AT&T and the University of Illinois for providing access to the beamline X16A and their hospitality during his visit in Brookhaven.

References

[1] I. Waller, Ann. Phys. 83 (1927) 153.

[2] W.F. Kuhs, Acta Cryst. A 48 (1992) 80.

[3] B.T.M. Willis, Acta Cryst. A 25 (1969) 277.

[4] B.T.M. Willis and A.W. Pryor, Thermal Vibrations in Crystallography (Cambridge University Press, Cambridge, 1975).

[5] U.H. Zucker and H. Schulz, Acta Cryst. A 38 (1982) 563.

[6] W.F. Kuhs, Acta Cryst. A 38 (1983) 148.

[7] P. Zeppenfeld, K. Kern, R. David and G. Comsa, Phys. Rev. Lett. 62 (1989) 63.

[8] L. Wenzel, D. Arvanitis, H. Rabus, T. Lederer and K. Baberschke, Phys. Rev. Lett. 64 (1990) 1765.

[9] M.A. Van Hove, W.H. Weinberg and C.-M. Chan, Low Energy Electron Diffraction, Vol. 6 of Springer Series in Surface Sciences (Springer, Berlin, 1986).

[10] R. Feidenhans'l, Surf. Sci. Rep. 10 (1989) 105; I.K. Robinson, in: Handbook of Synchrotron Radiation, Vol. 3, Eds. D.E. Moncton and G.S. Brown, Vol. 3 (North-Holland, Amsterdam, 1990).

[11] P.H. Fuoss and I.K. Robinson, Nucl. Instrum. Methods 222 (1984) 171.

[12] H.L. Meyerheim, J. Wever, V. Jahns, W. Moritz, P.J. Eng and I.K. Robinson, Surf. Sci. 304 (1994) 267.

[13] H.L. Meyerheim, Habilitation Thesis, Universität München, 1994.

[14] P.J. Eng, I.K. Robinson, H.L. Meyerheim and W. Moritz, unpublished.

[15] P. Bak, Rep. Prog. Phys. 45 (1982) 587.

[16] C.K. Johnson and H.A. Levy, in: International Tables for X-Ray Crystallography, Eds. J.A. Ibers and W.C. Hamilton, Vol. IV (Kynoch, Birmingham, 1974) p. 316.

[17] The agreement parameters R_u, R_w and GOF are defined as follows: $R_u = \Sigma_{hkl}||F_{hkl}^{obs}| - |F_{hkl}^{calc}||/\Sigma_{hkl}|F_{hkl}^{obs}|$; $R_w = (\Sigma_{hkl}w_{hkl}||F_{hkl}^{obs}| - |F_{hkl}^{calc}||^2/\Sigma_{hkl}w_{hkl}|F_{hkl}^{obs}|^2)^{1/2}$, with $w_{hkl} = \sigma_{hkl}^{-2}$; GOF $= (N-P)^{-1}\Sigma_{hkl}(||F_{hkl}^{obs}| - |F_{hkl}^{calc}||^2/\sigma_{hkl}^2)$, where N is the number of reflections and P the number of free parameters.

[18] A. Erdely, Higher Transcendental Functions, Vol. II (McGraw-Hill, New York, 1953).

[19] U.H. Zucker, E. Perenthaler, W.F. Kuhs, R. Bachmann and H. Schulz, J. Appl. Cryst. 16 (1983) 358.

[20] U.H. Zucker and H. Schulz, Acta Cryst. A 39 (1983) 148.

[21] See, e.g., W. Kleber, H.-J. Bautsch and J. Bohm, Einführung in die Kristallographie (Verlag Technik, Berlin, 1990).

[22] A.G. Naumovets and Yu.S. Vedula, Surf. Sci. Rep. 4 (1984) 365.